NIH-PA Author Manuscript

NIH-PA Author Manuscript

NIH-PA Author Manuscript

Multiple Roles of a Conserved GAF Domain Tyrosine Residue in Cyanobacterial and Plant Phytochromes[†]

Amanda J. Fischer[‡], **Nathan C. Rockwell[‡]**, **Abigail Y. Jang[‡]**, **Lauren A. Ernst[§]**, **Alan S. Waggoner[§]**, **Yong Duan[||]**, **Hongxing Lei[||]**, and **J. Clark Lagarias[*],[‡]**
Section of Molecular and Cellular Biology, University of California, Davis, California 95616, Department of Biological Sciences, Carnegie Mellon University, Pittsburgh, Pennsylvania 15213, and Department of Applied Sciences, University of California, Davis, California 95616

Abstract

The phytochrome family of red/far-red photoreceptors has been optimized to support photochemical isomerization of a bound bilin chromophore, a process that triggers a conformational change and modulates biochemical output from the surrounding protein scaffold. Recent studies have established that the efficiency of this photochemical process is profoundly altered by mutation of a conserved tyrosine residue (Tyr_{176}) within the bilin-binding GAF domain of the cyanobacterial phytochrome Cph1 [Fischer, A. J., and Lagarias, J. C. (2004) Harnessing phytochrome's glowing potential, *Proc. Natl. Acad. Sci. U.S.A. 101*, 17334–17339]. Here, we show that the equivalent mutation in plant phytochromes behaves similarly, indicating that the function of this tyrosine in the primary photochemical mechanism is conserved. Saturation mutagenesis of Tyr_{176} in Cph1 establishes that no other residue can support comparably efficient photoisomerization. The spectroscopic consequences of Tyr_{176} mutations also reveal that Tyr_{176} regulates the conversion of the porphyrin-like conformation of the bilin precursor to a more extended conformation. The porphyrin-binding ability of the $Tyr_{176}Arg$ mutant protein indicates that Tyr_{176} also regulates the ligand-binding specificity of apophytochrome. On the basis of the hydrogen-bonding ability of Tyr_{176} substitutions that support the nonphotochemical C15-*Z,syn* to C15-*Z,anti* interconversion, we propose that Tyr_{176} orients the carboxyl side chain of a conserved acidic residue to stabilize protonation of the bilin chromophore. A homology model of the GAF domain of Cph1 predicts a C5-*Z,syn*, C10-*Z,syn*, C15-*Z,anti* configuration for the chromophore and implicates Glu_{189} as the proposed acidic residue stabilizing the extended conformation, an interpretation consistent with site-directed mutagenesis of this conserved acidic residue.

Phytochromes are a widespread family of biliprotein photoreceptors specific for red and far-red light that were first identified in plants, where they modulate growth and development in response to changes in photosynthetically active radiation (*1–6*). Phytochromes and related photosensory proteins have also been identified in cyanobacteria, purple bacteria, nonphotosynthetic bacteria, and even fungi (*7–15*). Plant and microbial phytochromes incorporate linear tetrapyrrole molecules of different structures as their chromophores for sensing different shades of red and far-red light. Plant phytochromes (Phys)[1] employ phytochromobilin (PΦB), while cyanobacterial phytochromes (Cphs) use phycocyanobilin (PCB), the same pigment that is used by phycobiliproteins for light harvesting (*16–18*). The

[*] To whom correspondence should be addressed. Telephone: 530-752-1865. Fax: 530-752-3085. E-mail:jclagarias@ucdavis.edu..
[‡]Section of Molecular and Cellular Biology, University of California—Davis.
[§]Carnegie Mellon University.
[||]Department of Applied Sciences, University of California—Davis.

bacteriophytochromes from non-oxygenic photosynthetic and heterotrophic eubacteria (BphPs) instead make use of biliverdin IXα (BV), the more oxidized bilin precursor from which plant and cyanobacterial phytochrome chromophores are derived (*13*, *19–21*).

Absorption of a photon by the red-light-absorbing P_r form of phytochrome triggers the *Z–E* isomerization of the C15–C16 double bond of its bilin chromophore (*22*). This photoisomerization generates the spectrally distinct far-red-light-absorbing P_{fr} form, which can revert to P_r either upon absorption of a second photon or via a slow thermal process known as dark reversion. Numerous studies have established that the P_{fr} to P_r photoreversion reaction proceeds through spectrally distinct intermediates from the forward reaction (*23*, *24*). The interconversion between P_r and P_{fr} ultimately triggers a conformational change that alters the biochemical activity of phytochrome's C-terminal output region that is usually a protein kinase (*8*, *13*, *18*, *19*, *25–28*). For plant phytochromes, it is well-established that the N-terminal photosensory region transmits a second light signal via nuclear translocation and interaction with nuclear transcription factors (*29–31*). Phytochromes thereby transduce light signals via changes in gene expression, enabling long-term adaptation to changes in the light environment.

The photosensory input region of plant and microbial phytochromes typically consists of three evolutionarily related domains: a P2 domain that exhibits a weak homology to PAS domains, a P3 or bilin lyase domain recognized as a GAF domain, and a P4 or PHY domain [Figure 1A (*32*)]. Those phytochromes that employ BV, i.e., BphPs, possess a thioether linkage between the A-ring vinyl group of BV and a conserved Cys residue in the P2 domain (*15*, *20*, *21*, *33*), while plant and cyanobacterial phytochromes utilize more reduced bilin chromophores, i.e., PCB and PΦB, that are instead linked to a conserved Cys in the P3 domain (*16*, *18*). Interestingly, introduction of a Cys to the appropriate position in the P3 GAF domain of bacteriophytochromes permits covalent attachment of PCB (*33*, *34*), indicating that plant and microbial phytochromes have considerable structural similarity in their bilin-binding pockets.

It is generally accepted that the bilin prosthetic groups of phytochromes adopt semi-extended geometries *in situ*, but the overall conformation and protonation state of the P_r and P_{fr} chromophores has remained controversial until recently. Heteronuclear NMR spectroscopic analysis of the cyanobacterial phytochrome Cph1 from *Synechocystis* sp. PCC 6803 has established that the B/C-ring system of P_r and P_{fr} chromophores are both protonated (*35*), corroborating earlier vibrational spectroscopic investigations on plant phytochromes (*36*, *37*). Recent holoprotein assembly studies on Cph1 using stopped-flow spectroscopy indicate that PCB adopts a cyclic or porphyrin-like C5-*Z,syn*, C10-*Z,syn*, C15-*Z,syn* conformation upon initial binding to apoCph1 (*38*). This species rapidly interconverts to a more strongly red-light-absorbing, red-shifted intermediate that slowly transforms to the more blue-shifted P_r form upon thioether bond formation, the overall rate-limiting step for assembly (Figure 1B). A recent theoretical study suggests that the red shift of the extended, noncovalent intermediate is due to protonation of the chromophore ring system, while the increased oscillator strength of the visible transition reflects a more extended conformation (*39*). The extended conformation could involve adoption of a *Z,anti* configuration about C5, C15, or both, a conclusion that has received support from density functional theory calculations coupled with experimental resonanced Raman spectroscopy (*40*). Very recent work with synthetic, sterically locked BV

derivatives suggests that the P_r spectrum of an *Agrobacterium tumefaciens* BphP is best reproduced with a synthetic BV with a locked *Z,anti* configuration at C15, while a locked C15-*E,anti* BV analogue afforded an adduct resembling P_{fr} (*41*). When taken together, the simplest interpretation of these results and of the stopped-flow data is that the P_r chromophore possesses a C5-*Z,syn*, C10-*Z,syn*, C15-*Z,anti* configuration that arises from the initial porphyrin-like, all *syn* intermediate via a single, nonphotochemical *syn–anti* conformational interconversion (Figure 1).

Despite the current absence of a high-resolution phytochrome crystal structure, considerable indirect information is available for members of the phytochrome family in general and for the photosensory domains in particular. Truncation analysis has indicated that normal photochemistry does not require the C-terminal regulatory region (*15*, *42*, *43*). It is also possible to retain both covalent attachment of chromophore and photoconversion in the absence of the P4 or PHY domain, but such truncations exhibit reduced photoconversion efficiency, leading to the idea that this domain both stabilizes the core photosensory region (P2 and P3) and reduces futile de-excitation of the chromophore (*15*, *31*, *44*, *45*). Point mutants also have been isolated in the PHY domain that shift the absorbance spectrum without significantly affecting photochemistry (*46*), again indicating that this domain serves an accessory role. Deletion mutagenesis of the cyanobacterial phytochrome 2 (Cph2) has revealed that a P3 GAF domain alone is sufficient for PCB attachment (*45*). In apparent contrast, however, a 23 amino acid motif within the P2 PAS domain of AphA, a Cph1 orthologue from the cyanobacterium *Anabaena* sp. PCC 7120, was shown to play a critical role in holoprotein assembly (*47*). When these results are taken together, they indicate that phytochrome P3 GAF domains contain most of the chromophore contact sites important for reversible photochemistry, while the P2 and P4 domains perform more indirect roles in assembly and spectral tuning.

Our laboratory recently reported that mutation of conserved Tyr_{176} in the P3 GAF domain of Cph1 significantly increases the fluorescence yield of the holoprotein while inhibiting the P_r to P_{fr} photoconversion process (*46*). In that study, we hypothesized that this $Y_{176}H$ mutation reduced the rate of *Z–E* photochemical relaxation of the P_r excited state via a steric gating mechanism, thereby enhancing its fluorescence yield. The present study was undertaken to more fully examine the structural and functional role of this tyrosine residue. To determine whether this conserved tyrosine plays a similar role throughout the phytochrome family, we have introduced the Tyr-to-His mutation into representative plant phytochromes, full-length Cph1, and a representative bacteriophytochrome. Saturation mutagenesis of Tyr_{176} in Cph1 demonstrated a critical function of this tyrosine in maintaining the protonated, extended conformation of its bilin chromophore. To identify the potential proton donor, homology modeling of the Cph1 P3 GAF domain was performed. These results implicated Glu_{189}, a conserved acidic residue located near Tyr_{176}, in the stabilization of the protonated form of the B- and C-ring nitrogens of the bilin prosthetic group. To test this hypothesis, site-directed mutations of Glu_{189} were characterized, revealing a critical role for this residue in adoption of the extended conformation of the Cph1 chromophore.

MATERIALS AND METHODS

Plasmid Construction

The *Synechocystis* sp. PCC 6803 Cph1 plasmid pBAD-Cph1Δ and phycocyanobilin (PCB) biosynthetic plasmid pPL-PCB were previously described (*48*). The *Pseudomonas aeruginosa* PA 4117 BphP plasmids pASK-IBA2-PaBphP-ST (*21*) with and without the $Tyr_{163}His$ mutation were a gift from Nicole Frankenberg-Dinkel (University of Braunschweig, Germany). The pPL-PΦB plasmid that contains a synthetic operon consisting of the *Synechocystis* sp. PCC 6803 heme oxygenase ho1 (Cyanobase Locus SLL1184) and the *Arabidopsis* phytochromobilin synthase (HY2, NCBI Locus AB045112) fused to glutathione-

S-transferase (GST) in the expression vector pPRO-LarA122 (Clontech) was constructed as follows. Using the plasmid DNA template pGEX-mHY2 (*49*) that contains the full-length HY2 cDNA lacking the transit peptide fused to GST the GST-HY2 chimera was PCR-amplified with the primers GST-mHY2-*Eco*RV, 5′-CGGATATCATGTCCCC-TATACTA-3′, and mHY2-*Not*I, 5′-GCGCGGCCGCTTAGC-CGATAAATTGTCC-3′. The resulting PCR product was subcloned into plasmid pCR2.1/HO1-RBS (*48*) using *Eco*RV and *Not*I sites to produce plasmid pCR2.1/HO1-RBS-GSTHY2. The entire HO1-GSTHY2 operon from this plasmid was then subcloned into pPROLarA122 using *Kpn*I and *Not*I to produce pPL-PΦB. The full-length Cph1 plasmid pBAD-Cph1FL-myc/his was produced using pASK75B-Cph1-ST (*8*) as a PCR template with appropriate primers. The resulting PCR product was cloned into pBAD-myc/hisC (Invitrogen) with *Nco*I and *Hin*dIII. The Cph1-PAS/GAF truncation plasmid pBAD-Cph1(PAS/GAF)-myc/his was produced using pBAD-Cph1Δ (*48*) as a PCR template with the primers *Nco*IF-Cph1-P2, 5′-GGGCTAACAGGAGGAAT-TAACCATG-3,′ and *Pvu*IIR-Cph1-P3, 5′-CAATAAAAC-CGCTTCATGCTCCGCCAG-3′. The PCR product, encoding the N-terminal 350 amino acids of Cph1, was cloned into pBAD-myc/hisC with *Nco*I and *Pvu*II. pASK75B-AtPhyA(N599)-ST, encoding the N-terminal 599 amino acids of PHYA from *Arabidopsis*, was derived from the plasmid pA2a, a kind gift from Joanne Chory (Salk Institute, La Jolla, CA) by PCR using the primers 5′-CAGGATCCAGAAT-TCGAGCTCTC-3′ and 5′-GCGTCGACCGACCTTTGTAT-TCACATC-3′, and the PCR product was cloned into pASK75B-ST (*8*) with *Bam*H1 and *Sal*I. pBAD-AtPhyB-(N450)-6×his, encoding the N-terminal 450 amino acids of PHYB from *Arabidopsis* with a C-terminal His$_6$ tag, was derived from pBS-AtPhyB-ST, which was generated from the *Xba*I–*Kpn*I fragment of pYES2-AtPHYB-ST (*50*) and the similarly restricted pBluescript II KS+. The sequence corresponding to the N-terminal 450 amino acids was amplified using pBS-AtPhyB-ST and the primers AtBN450-(*Nco*I), 5′-CATGCCATGGCCGTTTCCGGAGTCGGGGG-TAG-3′, and AtBN450(*Eco*R1), 5′-GGAATTCCAGTGTCT-GCGTTCTCAAAACGCG-3′. The PCR product was cloned into the pBAD-myc/his-C vector using *Eco*RI and *Nco*I to produce pBAD-AtPhyB(N450)-6×his. QuikChange Site-Directed Mutagenesis (Stratagene) was used to generate all other site-specific mutations using 10 ng of dsDNA template with appropriate primers. All mutants and plasmid constructs derived from PCR reactions were confirmed by DNA sequencing (Davis Sequencing; http://www.davissequencing.com).

Recombinant Holophytochrome Expression and Purification

Phytochrome expressions for pASK-AtPhyA(N599)-ST and pASK-IBA2-PaBphP-ST were carried out as described (*21*). All other phytochrome expressions were performed in *Escherichia coli* strain LMG194 (Invitrogen) containing plasmids pPL-PCB or pPL-PΦB. Prior to expression, pPL-PCB- and pPL-PΦB-containing strains were maintained in minimal media (RM Media, Invitrogen) to repress expression of the bilin biosynthetic operon. Overnight precultures, in 3 mL of RM media containing 35 μg/mL kanamycin and 100 μg/mL ampicillin, were diluted 1:200 into 200 mL of the same medium and grown at 37 °C to an OD$_{580}$ of ~0.5. These cultures were transferred into 600 mL of Luria–Bertani medium containing 100 μg/mL ampicillin, 35 μg/mL kanamycin, and 1 mM isopropyl-β-D-thiogalactoside (IPTG). After incubation for 1 h at 37 °C, L-arabinose was added to a final concentration of 0.002% (w/v) (*48*). The cultures were then incubated overnight (~20 h) at 20 °C, after which cells were collected by centrifugation and resuspended in 5 mL of cold lysis buffer [50 mM Tris-HCl at pH 7.0, 300 mM NaCl, 10% (v/v) glycerol, 0.05% (v/v) Tween 20, 1 mM 2-mercaptoethanol, and 20 mM imidazole]. Cell suspensions were passed though a French pressure cell (⅜″ D) 3 times at 10 000 psi. Cell lysates were incubated with 10 units of DNase I (RNase-free, Fermentas) at room temperature for 10 min with moderate agitation followed by ultracentrifugation at 200000*g* for 30 min. The resulting crude soluble protein extracts were applied to Talon metal-affinity spin columns (1 mL of bed volume, BD Biosciences) that had

been pre-equilibrated with 3 mL of lysis buffer. Columns were then washed with 3 mL of lysis buffer, and bound protein was eluted with 2 mL of elution buffer (lysis buffer and 200 mM imidazole). Eluates were diluted 1:5 with protein buffer [25 mM Tes KOH at pH 7.5 and 10% (v/v) glycerol], passed through a 0.45 μm Acrodisc syringe filter (Gelman Sciences), and applied to a HiTrap Q HP anion-exchange column (1 mL of bed volume, Amersham Biosciences) pre-equilibrated with protein buffer. Columns were washed once with protein buffer containing 0.1 M NaCl (5 mL), and the recombinant protein was then eluted with protein buffer containing 0.5 M NaCl. Eluates were exchanged into protein buffer using an Amicon Ultra-4 Centrifugal Filter with a 30000 Da nominal molecular-weight limit, flash-frozen in liquid nitrogen, and stored at −80 °C.

Cyanogen Bromide Digestion and Chromopeptide Isolation

Approximately 100–200 μg of the purified Cph1Δ-PCB and Cph1Δ ($Y_{176}R$)-PCB holoproteins were dialyzed into 50 mM ammonium acetate (pH 7.5) overnight at 4 °C. Protein solutions were then evaporated to ~25 μL in a Speedvac concentrator (Savant) and redissolved in 100 μL of deionized water. This solution was evaporated to dryness and dissolved in 60 μL of 70% aqueous TFA containing 2 M cyanogen bromide for protein digestion. Samples were incubated at room-temperature overnight in darkness to allow for complete digestion. These solutions were then dried under a stream of nitrogen gas, dissolved in 200 μL of 20% formic acid, and applied to a reversed-phase HPLC column (250 × 4.6 mm, Jupiter 4μ Proteo 90Å, Phenomenex). Peptides were eluted at 1 mL/min with a water/acetonitrile gradient in 20 mM formic acid. Absorbance was monitored at 220, 400, and 650 nm.

SDS–PAGE and Zinc-Blot Analysis

Protein samples were analyzed using 10% SDS–PAGE with the Laemmli buffer system (*51*). Zinc-blot analysis was carried out as described previously (*52*, *53*).

Absorbance and Fluorescence Spectroscopy

Absorbance and difference spectra were obtained using a HP8453 UV–visible spectrophotometer (*48*). Red (650 ± 5 nm) and farred (720 ± 5 nm) light with fluence rates of >100 μmol m^{-2} s^{-1} were used for effecting phytochrome photoconversion, with sufficient duration of irradiation to ensure completeness. Fluorescence excitation and emission spectra were obtained with an SLM Aminco Bowman AB2 fluorimeter with both monochromators adjusted to a 4 nm bandpass. Fluorescence quantum yield measurements were determined with a Photon Technology International, Inc., SE 901M spectrofluorometer using purified cyanine dye (CY-5.18) as a standard as described previously (*46*, *54*, *55*).

Homology Modeling of Cph1 P3 Bilin Lyase Domain

An initial model for the P3 GAF region of Cph1, comprising amino acids 151–322 in the full-length sequence, was generated using 1MC0 (*56*) as a template with side-chain conformations generated by SCRWL (*57*). The region connecting the fourth and fifth strands (Asp_{226}–Gly_{270}) was poorly aligned to the template (see Supplemental Figure 1 in the Supporting Information). Therefore, the structure in this region was built manually. Inspection of the hydrophobic pattern suggested that the segment between Ser_{241} and His_{260} could be an amphipathic α helix. When this helix was docked to the rest of the template structure, the hydrophobic surface could be buried and isolated from the solvent. Furthermore, the helix also allowed Cys_{259} to point toward the conserved residue Tyr_{176}. Two linker segments were then added to connect the helix to the main template. This structure was refined in explicit solvent for 200 ps using AMBER, during which a short helix between Asp_{226} and Val_{232} was formed. The resulting structure served as the initial model.

To create a model incorporating chromophore, Merz–Kollman partial charges were calculated for PCB at the HF/6-31G level of theory using Gaussian 98 Revision A.9 (*58*) and assuming that the endo-vinyl side chain of the A ring had been reduced to mimic the situation after covalent attachment of the Cys residue. The resulting charges for the B/C-ring system were then scaled to a total of +1 for incorporation into the GROMOS96 43a1 and AMBER parameter sets (*59*, *60*), and appropriate examples from these force fields were chosen for the remaining partial charges and other parameters. Parametrization of PCB in the 43a1 force field was sufficient to permit stable simulation of free PCB in explicit solvent using Gromacs 3.2 (*61*).

PCB was then manually docked into the protein model using VMD (*62*) with the following four assumptions: one, the propionate side chains of PCB were more likely to be exposed to the solvent than the more hydrophobic PCB ring system; two, the register of the first and second β strands was chosen to place highly conserved residues (including Tyr_{176}) facing the presumptive chromophore-binding pocket; three, the stereocenter generated by the Cys–PCB bond should be in the *R* configuration, by analogy to plant phytochrome (*16*); and four, the P_r form of PCB should be protonated on both B and C rings with the C15–C16 double bond in the *Z* configuration. Brief (0.1 ps) molecular dynamics simulations in Gromacs or AMBER were used to relieve strain introduced during docking. After initial docking, rotation of either the A or D ring was considered as alternative means of generating the extended P_r conformation of PCB. Rotation of the A ring while retaining proper *R* stereochemistry implied either burial of the PCB carboxylates in an unfavorable hydrophobic environment or adoption of a strained A-ring geometry that was not maintained during simulation (data not shown). In contrast, rotation of the D ring readily permitted retention of stereochemistry with burial of the more hydrophobic ring system and exposure of the propionate side chains to the solvent; therefore, this configuration was chosen as the basis for further refinement. The resulting holoprotein models were subjected to longer molecular dynamics simulations in AMBER or Gromacs to generate two configurations each having favorable and unfavorable aspects.

On the basis of sequence homology and the expectation that the chromophore-ring system should be largely excluded from the solvent to favor photochemistry, these models were combined into a single apoprotein model using MODELLER version 8.0 (*63*). The resulting model was then further refined by shifting the register of the sixth β strand with MODELLER to place a conserved Trp residue in the interior to account for observed energy transfer between chromophore and a tryptophan (*64*). This was followed by subsequent 0.1 ps simulation in Gromacs and finally by generation of several possible configurations for the loop between the second and third β strands with MODELLER. One of these loops was chosen as offering the best burial of PCB, and this model was then subjected to 1.2 ns of simulation time in Gromacs, with the last 400 ps giving little change in the model structure. The final model conforms to the four assumptions stated above and predicts that the P_r configuration of Cph1 should adopt a C5 *Z,syn*, C10 *Z,syn*, C15 *Z,anti* conformation.

To model a cyclic conformation as observed during the Cph1–PCB assembly reaction (*38*), partial charges were calculated for PCB as described above with deprotonation of either the B or C ring. The resulting partial charges were then slightly adjusted (≤ 10%) such that the total charge on the B/C-ring system was approximately 0 and were then incorporated into the 43a1 force field to give two deprotonated tautomers. The final model for protonated chromophore was manually modified in VMD to restore the porphyrin-like configuration observed upon initial binding of PCB to Cph1 (i.e., C5 *Z,syn*, C10 *Z,syn*, C15 *Z,syn*, Figure 1). The complexes between Cph1 and both deprotonated PCB tautomers were modeled as covalent holoproteins, because the present study demonstrates that the cyclic chromophore configuration is compatible with covalent attachment. The resulting complexes were subjected to 1 ns simulations in Gromacs with explicit protonation of Glu_{189} as the most obvious candidate proton donor in our model. Apoprotein was similarly modeled by editing the holoprotein PDB

file to remove PCB and then carrying out 1 ns of simulation with Gromacs. Figures were prepared using VMD (*62*), Tachyon (*65*), STRIDE (*66*), and Adobe Photoshop CS (Adobe Systems, Inc.). Preparation of Supplemental Figure 1 in the Supporting Information also used STAMP (*67*), CLUSTALW (*68*), and homolmapper (N. C. Rockwell and J. C. Lagarias, unpublished results).

Theoretical pK_a Calculations

pK_a calculations were performed using MEAD and Redti (*69*) on six snapshots taken at 20 ps intervals across the last 100 ps of the trajectories to compensate for slight variations in the structure during molecular dynamics. For MEAD calculations, changes in the ionization state of the PCB-ring system (and hence site–site interactions between the PCB-ring system and titrating groups on the protein) were neglected because the pK_a value for the ring system in isolated PCB is itself ill-defined and because the errors incorporated in the current homology model seem likely to be at least as significant for this application. pK_a calculations were performed on apoprotein (mean pK_a for Glu$_{189}$, 4.4 ± 0.7), deprotonated PCB (8.1 ± 1.0 and 7.4 ± 1.2 for the tautomers with B and C ring deprotonated, respectively) and protonated PCB (−1.4 ± 1.2) with explicit consideration of ionization for all Asp, Glu, His, Lys, Arg, Cys, and Tyr residues except for Cys$_{259}$, which was covalently attached to PCB and thus was nontitrating. The ionization of the PCB propionate moieties was also explicitly included in the calculation. The non-physiological pK_a value for protonated chromophore is likely to indicate that protonation of Glu$_{189}$ in the context of protonated chromophore will cause structural change (*70*).

RESULTS

Tyr$_{176}$ and Its Equivalents Perform a Conserved Photochemical Function in Plant and Cyanobacterial Phytochromes

The demonstration that a single amino acid substitution at a conserved position in the GAF domain (Y$_{176}$H) was sufficient to evolve Cph1 into a fluorescent protein (*46*) led us to ask whether this was a phenomenon unique to Cph1 or reflected an inherent property of phytochromes in general. To examine this question, a construct expressing the N-terminal 450 amino acids of PhyB from *Arabidopsis* [equivalent to the P1–P2–P3 domains (*31*)], with or without the equivalent Y$_{276}$H mutation, was expressed and purified from PCB-producing *E. coli* cells (*48*). Like the Y$_{176}$H mutant of Cph1Δ, the corresponding AtPhyB-(N450) mutant exhibited enhanced fluorescence and reduced efficiency of photoconversion (<10% of the wild type, Figure 2). Similar results were observed for an *Arabidopsis* phytochrome A Y$_{242}$H mutant holoprotein containing the entire photosensory domain (data not shown). Because plant phytochromes use PΦB instead of PCB, we examined the influence of chromophore substitution in the YH mutant. PΦB adducts of both Cph1Δ and AtPhyB(N450) YH mutant proteins yielded fluorescent proteins with reduced photoconversion efficiencies, indicating that the enhanced fluorescence is not specific for the PCB chromophore (Supplemental Table 1 in the Supporting Information and data not shown). We also examined the corresponding Y$_{163}$H mutation in the *Pseudomonas aeruginosa* bacterial phytochrome PaBphP, which unusually exhibits a P$_{fr}$ spectrum at the thermal ground state (*21*). In this case, the wild-type holoprotein BV adduct exhibited considerable fluorescence, as has also recently been reported for multiple bacteriophytochromes from *Rhodopseudomonas palustris* (*28*), but the Y$_{163}$H mutant PaBphP protein exhibited no fluorescence enhancement (data not shown). When these results are taken together, they indicate that the conserved P3 GAF domain tyrosine residue performs a similar photochemical gating role in plant (Phy) and cyanobacterial (Cph1) phytochromes but plays a distinct role in bacteriophytochromes.

The $Y_{176}H$ mutation in Cph1 was also analyzed both in full-length Cph1 and in a more truncated Cph1 consisting of only the N-terminal P2 PAS and P3 GAF domains (approximately equivalent to AtPhyBN450), to assess the possibility that the novel spectroscopic properties were due to altered protein folding of the specific truncation constructs tested. In both cases, the $Y_{176}H$ mutation resulted in reduced photoconversion and increased fluorescence compared with its WT counterpart (data not shown). The $Y_{176}H$ mutant derived from the Cph1 PAS/GAF construct had a reduced fluorescence quantum yield (0.083) compared with the Cph1Δ mutant (0.145). This suggests that more energy is lost through futile modes of de-excitation upon removal of the PHY domain, a result consistent with earlier studies (*45*).

Tyr$_{176}$ Is Essential for Normal Cph1 Photochemistry

To assess the range of possible phenotypes associated with the mutation of Tyr_{176}, saturation mutagenesis of this residue was performed. All amino acid substitutions at this position resulted in soluble covalently bound biliproteins except for the proline mutant, which was poorly expressed (Supplemental Figure 2 in the Supporting Information). These results indicate that Tyr_{176} is not required for proper apoprotein folding or chromophore attachment. All of the purified Tyr_{176} mutant proteins exhibited reduced photoconversion efficiencies as measured by difference spectroscopy with the next most photoactive substitution mutants, i.e., $Y_{176}S$ and $Y_{176}T$, exhibiting 34 and 13% of the wild-type photoconversion efficiency, respectively (Table 1). Tyr_{176} is thus necessary for optimal photochemistry. The reduced difference spectra could indicate that the forward reaction (P_r to P_{fr}) is specifically affected by mutation of Tyr176, which seems plausible because the reverse reaction proceeds through different intermediates and is thus a distinct pathway (*23*, *24*), that the P_r and P_{fr} forms of the mutant proteins have indistinguishable spectra or that the conversion to P_{fr} has become so energetically disfavorable that the contribution of the reverse reaction to the measured difference spectra is negligible. We have not attempted to discriminate between these possibilities.

In addition to the $Y_{176}H$ substitution, three other amino acid substitutions conferred enhanced fluorescence upon Cph1Δ, i.e., Gln, Glu, and Trp (Table 1). These four mutant proteins exhibited fluorescence emission maxima ranging from 671 to 681 nm as PCB adducts; all four mutants were poorly photoactive. $Y_{176}H$ was the most fluorescent as determined by quantum yield measurements (Table 1). Enhanced fluorescence was also observed for their PΦB adducts; however, in comparison with the corresponding PCB adducts, all such mutants had reduced fluorescence quantum yields and red-shifted fluorescence emission maxima except for $Y_{176}W$, which resulted in a PΦB adduct with a similar fluorescence quantum yield to the PCB adduct (Supplemental Table 1 in the Supporting Information).

Tyr$_{176}$ Is Required for the Protonated, Extended Chromophore Conformation

All substitutions at position 176 led to a reduction in the red/blue absorbance ratio, indicating that the bilin prosthetic group is bound to the mutant proteins in a more cyclic conformation [Figure 3A and Table 1 (*39*, *71*)]. Additionally, all Tyr_{176} mutant proteins displayed blue-shifted absorbance maxima for the long wavelength transition (Table 1). A plot of the blue shift versus the R/B ratio demonstrated a correlation between a decreasing R/B ratio and an increasing blue shift, with the R/B ratio decreasing from that of wild-type Cph1Δ (R/B ratio > 3) to an apparent minimum ratio of approximately 0.5 (Figure 3B). Interestingly, mutants exhibiting enhanced fluorescence or relatively efficient photoconversion had the largest R/B ratios, with the exceptions being $Y_{176}W$ and $Y_{176}T$ (Table 1). Extended chromophore conformations therefore also correlate with de-excitation of the excited state via either photoconversion or fluorescence, reflecting minimized excited-state decay through nonproductive, radiationless pathways. Intermediate cases may reflect the presence of two populations within the purified preparation: a population with extended chromophore, which

is competent for photoconversion and has a high R/B ratio, and a population with cyclic chromophore, which is incompetent for photoconversion and has a low R/B ratio.

Previous stopped-flow studies of apoCph1 assembly demonstrated that the chromophore of the Cph1·PCB complex converts from a porphyrin-like conformation to a more extended conformation prior to covalent attachment [Figure 1 (*38*)]. The authors of this work proposed that this conformational interconversion reflects protonation of both B/C-ring system pyrrole nitrogens of the bilin chromophore, by analogy to the pH dependence of free bilin spectra (*71*). This interpretation is also consistent with recent NMR data showing that all four PCB nitrogens are protonated in the P_r state (*35*). Protonation and isomerization of the chromophore thus seem to be coupled processes both in solution and in the phytochrome-binding pocket, with covalent attachment occurring more slowly than chromophore isomerization. Because most of the Tyr_{176} mutant proteins have covalently attached chromophores with R/B absorbance ratios consistent with the cyclic deprotonated conformation, our results suggest that chromophore protonation is not a prerequisite for covalent bond formation. It should be noted that these mutant proteins are assembled into holoproteins over a 20 h period. For this reason, we cannot rule out that deprotonation occurs following chromophore attachment. When these data are taken together, they demonstrate that Tyr_{176} is required for maintenance of the extended, protonated conformation of the chromophore.

The $Y_{176}R$ Mutant Binds an Endogenous Porphyrin

In contrast to wild-type Cph1 and all other Tyr176 mutant proteins, the $Y_{176}R$ mutant surprisingly exhibited an absorbance spectrum with features of a nonbilin pigment. On the basis of an intense 400 nm absorbance maximum and the fluorescence excitation/emission spectra (Figure 4), it was clear that a porphyrin was associated with this mutant. However, the broader absorbance maximum at longer wavelengths (~623 nm, Figure 4) suggested that the purified protein also contained a bilin chromophore, indicating that the purified preparation consisted of two populations with different chromophores. To assess whether the porphyrin was covalently attached, wild-type and $Y_{176}R$ proteins were digested with CNBr and the resulting peptide mixture was separated by reverse-phase HPLC. Two chromopeptides were observed, one eluting at the same time as the single wild-type Cph1Δ chromopeptide and a second eluting 1.5 min later (Supplemental Figure 3 in the Supporting Information). The absorbance spectrum of the former was similar to the PCB-bound chromopeptide derived from wild-type Cph1Δ, while the absorbance spectrum of the second chromopeptide clearly demonstrated a bound porphyrin. These results indicated that the $Y_{176}R$ mutation altered the chromophore specificity of Cph1Δ, apparently enabling an endogenous porphyrin to covalently bind to the apoprotein. The chemical structure and linkage of this bound porphyrin is the subject of an ongoing investigation.

Homology Modeling Predicts Close Association of Tyr_{176} and Glu_{189} in the P3 Domain of Cph1

To develop hypotheses concerning the role of Tyr_{176} in chromophore protonation, we generated homology models of the Cph1 P3 bilin lyase domain using published crystal structures of GAF domains as templates (*56, 72, 73*). Using a multiple sequence alignment with both GAF domains of mouse phosphodiesterase 2A (PDB ID 1MC0, Supplemental Figure 1 in the Supporting Information), a homology model of the Cph1 P3 domain predicted a six-stranded, antiparallel β-sheet scaffold with helices on either side (Figure 5A). Because there is little sequence identity within the phytochrome family in the large insert between the fourth and fifth β strands, substantial refinement of this region was not undertaken. The resulting model placed several residues conserved among phytochromes about a central cavity that is likely to constitute the chromophore-binding pocket.

We then manually docked PCB chromophore into this pocket and carried out additional refinement as described in the Materials and Methods. The final model was subjected to 1.2 ns of molecular dynamics simulation in explicit solvent in Gromacs 3.2.1 (*61*). The resulting model stably incorporates PCB into the proposed chromophore-binding pocket; PCB is predicted to assume the C5-*Z*,*syn*, C10-*Z*,*syn*, C15- *Z*,*anti* configuration in the P_r form (Figure 1), while also maintaining the stereochemistry of the Cys–PCB linkage based on that of plant phytochromes (*16*). This model also exhibited a number of favorable interactions between PCB and highly conserved protein residues (Figure 5 and Supplemental Figure 1 in the Supporting Information). In particular, the Tyr_{176} side chain lies within 3.5 Å of both the C_{15} methine bridge and the D-ring methyl group (Figure 5B). This model also predicts that Tyr_{176} is hydrogen-bonded to the carboxyl side chain of Glu_{189} (Figure 5B). Because Glu_{189} can form multiple hydrogen bonds with the positively charged B/Cring system of the protonated chromophore in this model (Figure 5C), its involvement in stabilizing the charge of the protonated chromophore appeared reasonable.

Glu_{189} Is Required for Chromophore Protonation

To test the hypothesis that Glu_{189} is required to stabilize the protonated, extended chromophore conformation, this residue was mutated to Gln and Ala. A previous study utilizing a short *in vitro* assembly reaction had shown this residue to be essential for holoprotein formation, but we hoped that *in vivo* assembly would permit assembly of Glu189 mutant holophytochromes. Indeed, the two Glu_{189} mutations yielded soluble holophytochromes with bound chromophore (Supplemental Figure 2 in the Supporting Information), which exhibited highly reduced photoconversion efficiencies (4% for $E_{189}A$ and 10% for $E_{189}Q$, Table 1). Both Glu_{189} mutants displayed significantly reduced red/blue ratios, consistent with their chromophores adopting cyclic conformations (Table 1). The long wavelength absorbance band was also blue-shifted with both mutant proteins (Figure 3B, □), indicating that the mutation of Glu_{189} resulted in comparable effects to the mutation of Tyr_{176}.

DISCUSSION

The data that we present here demonstrate that the conserved Tyr_{176} in the P3 domain of Cph1 plays a key role in the structure and function of holophytochromes. First, the gain-of-function fluorescence observed in the $Y_{176}H$ mutant of Cph1 (*46*) is also observed in at least two plant phytochromes upon introduction of the equivalent mutation. This gain-of-function fluorescence is observed with both PΦB and PCB chromophores, indicating that the spectral gating function of the P3 GAF domain Tyr is similar for both bilin chromophores. Moreover, we show that Tyr_{176} is essential for optimal photoconversion; no other residue supports even 50% of wild-type levels of photoconversion to P_{fr}. Indeed, the most conservative substitution (i.e., $Y_{176}F$) is among the least photoconvertible, i.e., 3% of the wild type (Table 1). Our studies show that Tyr_{176} is critical for adoption of the extended, protonated P_r chromophore conformation, because many mutant proteins instead covalently bind chromophore in a cyclic, deprotonated conformation reminiscent of a porphyrin (Figure 3). In the most extreme example of this altered conformational specificity, substitution of Arg for Tyr at this position resulted in a mutant phytochrome that preferentially bound a porphyrin (Figure 4 and Supplemental Figure 3 in the Supporting Information).

The increased fluorescence associated with mutation of Tyr_{176} in both Cph1 and plant phytochromes indicates that this residue has a conserved role in the photochemical interconversion of P_r to the primary intermediate Lumi-R (*46*). Both Cph1 and plant phytochromes are known to exhibit de-excitation on a subnanosecond time scale with their native chromophores (*74, 75*). Use of the alternative chromophore phycoerythrobilin, which has a saturated C15 methine bridge, extends the excited-state lifetime into the nanosecond time

scale, leading to enhanced fluorescence (*75, 76*). By analogy, the mutation of Tyr_{176} or the equivalent residue in plant phytochromes could prevent the normal path of photoreaction and prolong the lifetime of the excited state, resulting in increased fluorescence.

Interestingly, the introduction of the equivalent $Y_{163}H$ mutation into the bacteriophytochrome PaBphP did not result in a comparable enhancement of fluorescence. This indicates that there must be differences in the chromophore–protein interactions and/or photochemical reaction pathways of the BphP subfamily relative to plant and cyanobacterial phytochromes. In contrast to the very low fluorescence observed with wild-type Cph1 or plant phytochrome (Table 1), wild-type bacteriophytochromes RpBphP2 and RpBphP3 from *R. palustris* both exhibit substantial fluorescence in the P_r state (*28*), as did wild-type PaBphP in our hands (data not shown). These results suggest that members of the BphP subfamily may have an intrinsically higher P_r fluorescence and hence a longer excited-state lifetime for photoconversion from P_r to P_{fr} compared with plant (Phy) and cyanobacterial (Cph1) phytochromes. Mutation of this conserved Tyr residue apparently does not have a comparable effect on the BphP excited-state lifetime.

The current study does not fully elucidate the role(s) of Tyr_{176} in the photochemistry of Cph1. On the basis of current data, the proposal that this residue is involved in sterically gating the P_r to P_{fr} transition (*46*) is still plausible. Indeed, the contacts between PCB and Tyr_{176} in the current homology model are consistent with such a role, although this model is unlikely to be accurate in atomic detail. In the present study, we show that four residues resulted in a significant increase in fluorescence when substituted for Tyr at position 176: His, Gln, Glu, and Trp (Table 1). All of these residues possess potential hydrogen-bonding donor/acceptor side chains that are positioned four atoms removed from the peptide backbone. As we proposed earlier (*46*), a fortuitous hydrogen bond with the bilin chromophore, another residue in the PCB-binding pocket, or even water could account for an increased activation barrier for photochemical de-excitation of the P_r excited state. The molecular basis for the fluorescence enhancement may differ between the four mutants. Introduction of the large Trp residue at position 176 might inhibit rotation of the D ring on steric grounds, while the other mutations may enhance D-ring rigidity via a different mechanism(s). The reduced R/B ratio seen with $Y_{176}W$ relative to the other fluorescent mutant proteins (Figure 3B) is consistent with this interpretation. Further studies, especially those that generate experimental structural information, are needed to more fully understand the structural basis of the fluorescence enhancement.

Our data also show that Tyr_{176} is important for the adoption of the normal P_r chromophore conformation. Many substitutions at this position result in a holoprotein in which the chromophore exhibits a slight blue shift and a substantially lower R/B ratio, indicative of a chromophore in a cyclic configuration (*71*). Gas-phase calculations suggest that the red enhancement observed during formation of wild-type P_r holoprotein is the direct consequence of rotation about the C5 or C15 methine bridges, while the red shift of the absorbance maximum is the consequence of protonation of the B/C-ring system pyrrole nitrogens (*39*). Our mutant proteins show a rough correlation between these two spectral trends (Figure 3B). While the R/B ratio reaches an apparent minimum value that would presumably be expected for the cyclic conformation, it is unclear whether the value observed for the wild type reflects a maximum. Moreover, the mutants that have a minimal R/B ratio exhibit a range of absorbance maxima. It thus seems likely that our current spectral data reflect the presence of two species: a cyclic, deprotonated form that predominates in most of the mutant proteins and an extended, protonated form that predominates in wild-type Cph1. Our data thus show that Tyr_{176} is an important residue both for the adoption of the proper chromophore configuration and for photoconversion, perhaps indicating overlap between the structural changes involved in assembly of holoprotein and those associated with the photochemical cycle.

The simplest explanation for the reduced R/B ratios of the different Tyr_{176} mutant proteins is that they reflect varying degrees of chromophore protonation, because protonation strongly favors formation of the extended C15 *Z,anti* conformation of the bilin chromophore (*71*). This implicates Tyr_{176} as critical for stabilization of the protonated state of PCB either via direct interaction with the proton donor itself or via its ability to optimally position an anionic residue near the B/C-ring positive charge. By analogy with the role of aspartate residues in stabilizing the protonated state of bilin chromophores in phycocyanin (*77, 78*), we reason that a residue with a carboxyl side chain would best fulfill this role in phytochrome. On the basis of previous studies indicating that the invariant acidic residue Glu_{189} is critical for chromophore attachment (*45*) along with homology modeling in the present study, this residue is a plausible candidate for maintaining the extended, protonated conformation of the Cph1 chromophore. Indeed, this hypothesis is consistent with the spectroscopic properties of the $E_{189}A$ and $E_{189}Q$ mutants, whose chromophores adopt porphyrin-like conformations. In view of the many assumptions made in developing our homology model, however, it remains possible that another conserved acidic residue within the GAF domain, e.g., Asp_{207} or Asp_{226}, could perform this role.

While the identity of the actual proton donor responsible for triggering the C15,*syn* to C15,*anti* conformational rearrangement is conceivably the same acidic residue that stabilizes the protonated chromophore, we cannot conclude this with certainty. Our homology model implicates His_{260} or Glu_{189} as the most likely candidates to fulfill this role. His_{260} is conserved, and the participation of His residues in proton-transfer reactions is well-documented in many protein systems. In our model, however, His_{260} lies closer to the A ring and thus appears better suited to mediate thioether attachment. In contrast, Tyr_{176} and Glu_{189} are more closely associated with the bilin B and C rings. Because the pK_a for a tyrosine phenol side chain is normally too high to play a significant role in such a proton transfer, Glu_{189} is the more reasonable candidate. However, the pK_a values for isolated Glu side chains are typically <5, indicating that the pK_a of Glu_{189} would have to be significantly increased for this residue to be a viable proton donor. Such increases for Glu pK_a values are not unknown; for instance, Glu_{35} in lysozyme has a pK_a value >6 (*79–81*). Initial attempts to estimate the Glu_{189} pK_a using the MEAD software suite (*69*) and the current model structure indicate that this residue has a normal pK_a in the apoprotein, a substantially elevated pK_a in the proposed apoprotein/PCB intermediate complex (protonated Glu_{189} with one proton on either the B or C ring of PCB), and a substantially decreased pK_a in the holoprotein complex depicted in Figure 5 (data not shown). While these calculations are likely to incorporate significant systematic error, they do suggest that Glu_{189} is a viable candidate for proton transfer to PCB during holoprotein assembly.

This hypothesis led us to examine the role of Glu_{189} in Cph1's assembly and photochemistry. This residue had previously been shown to be required for formation of holoprotein in a short *in vitro* assembly assay (*45*), but we reasoned that the *in vivo* expression system used in the present study might permit successful synthesis of the holoprotein. Indeed, both $E_{189}Q$ and $E_{189}A$ Cph1 were isolated as holoproteins, and both exhibited spectra consistent with cyclic, deprotonated chromophore configurations (Table 1). Mutation of Glu_{189} also ablated normal P_r to P_{fr} photoconversion. It thus appears that Glu_{189}, like Tyr_{176}, is required for the formation of the extended, protonated P_r chromophore conformation. In the absence of a crystal structure for any phytochrome, it is difficult to determine the precise mechanistic basis for the observed roles of these two residues in the photochemistry of Cph1 and plant phytochromes. However, the data presented here establish that both Tyr_{176} and Glu_{189} are required for the chromophore to adopt the extended, protonated C15, *Z,anti* conformation found in wild-type Cph1. Both residues are also required for efficient photoconversion. It will be interesting to see whether this correlation reflects actual similarities between the initial assembly pathway of holoprotein assembly and the phytochrome photocycle. During the wild-type photocycle, we hypothesize

that the orientation of these two residues is likely to change, a process that is likely to underlie the transmission of the light signal.

SUPPORTING INFORMATION AVAILABLE

(Supplemental Figure 1) Additional information about the sequence alignment used in homology modeling and the chromophore–protein interactions predicted by the resulting model. (Supplemental Figure 2) Purified mutant proteins reported in this paper. (Supplemental Figure 3) Chromopeptide analysis of the wild-type and $Y_{176}R$ Cph1. (Supplemental Table 1) Additional spectral information for those Tyr176 mutations that resulted in fluorescent holoproteins. This material is available free of charge via the Internet at http://pubs.acs.org.

References

1. Smith H. Phytochromes and light signal perception by plants—An emerging synthesis. Nature 2000;407:585–591. [PubMed: 11034200]

2. Schäfer, E., and Nagy, F., Eds. (2005) Photomorphogenesis in Plants and Bacteria: Function and Signal Tranduction Mechanisms, 3rd ed., pp 667, Springer Publishers, Dordrecht, The Netherlands.

3. Nagy F, Schäfer E. Phytochromes control photomorphogenesis by differentially regulated, interacting signaling pathways in higher plants. Annu Rev Plant Biol 2002;53:329–355. [PubMed: 12221979]

4. Quail PH. Phytochrome photosensory signalling networks. Nat Rev Mol Cell Biol 2002;3:85–93. [PubMed: 11836510]

5. Chen M, Chory J, Fankhauser C. Light signal transduction in higher plants. Annu Rev Gen 2004;38:87–117.

6. Franklin KA, Whitelam GC. Light signals, phytochromes, and cross-talk with other environmental cues. J Exp Bot 2004;55:271–276. [PubMed: 14673030]

7. Kehoe DM, Grossman AR. Similarity of a chromatic adaptation sensor to phytochrome and ethylene receptors. Science 1996;273:1409–1412. [PubMed: 8703080]

8. Yeh KC, Wu SH, Murphy JT, Lagarias JC. A cyanobacterial phytochrome two-component light sensory system. Science 1997;277:1505–1508. [PubMed: 9278513]

9. Hughes J, Lamparter T, Mittmann F, Hartmann E, Gärtner W, Wilde A, Börner T. A prokaryotic phytochrome. Nature 1997;386:663. [PubMed: 9109482]

10. Jiang ZY, Swem LR, Rushing BG, Devanathan S, Tollin G, Bauer CE. Bacterial photoreceptor with similarity to photoactive yellow protein and plant phytochromes. Science 1999;285:406–409. [PubMed: 10411503]

11. Davis SJ, Vener AV, Vierstra RD. Bacteriophytochromes: Phytochrome-like photoreceptors from nonphotosynthetic eubacteria. Science 1999;286:2517–2520. [PubMed: 10617469]

12. Herdman M, Coursin T, Rippka R, Houmard J, de Marsac NT. A new appraisal of the prokaryotic origin of eukaryotic phytochromes. J Mol Evol 2000;51:205–213. [PubMed: 11029065]

13. Giraud E, Fardoux J, Fourrier N, Hannibal L, Genty B, Bouyer P, Dreyfus B, Verméglio A. Bacteriophytochrome controls photosystem synthesis in anoxygenic bacteria. Nature 2002;417:202–205. [PubMed: 12000965]

14. Idnurm A, Heitman J. Light controls growth and development via a conserved pathway in the fungal kingdom. PLoS Biol 2005;3:e95. [PubMed: 15760278]

15. Karniol, B., and Vierstra, R. D. (2005) Structure, function, and evolution of microbial phytochromes, in Photomorphogenesis in Plants (Schafer, E., Ed.) Martinus Nijhoff Publishers, Dordrecht, The Netherlands.

16. Lagarias JC, Rapoport H. Chromopeptides from phytochrome. The structure and linkage of the P_r form of the phytochrome chromophore. J Am Chem Soc 1980;102:4821–4828.

17. Wu SH, McDowell MT, Lagarias JC. Phycocyanobilin is the natural precursor of the phytochrome chromophore in the green alga *Mesotaenium caldariorum*. J Biol Chem 1997;272:25700–25705. [PubMed: 9325294]

18. Hübschmann T, Börner T, Hartmann E, Lamparter T. Characterization of the Cph1 holo-phytochrome from *Synechocystis* sp. PCC 6803. Eur J Biochem 2001;268:2055–2063. [PubMed: 11277928]

19. Bhoo SH, Davis SJ, Walker J, Karniol B, Vierstra RD. Bacteriophytochromes are photochromic histidine kinases using a biliverdin chromophore. Nature 2001;414:776–779. [PubMed: 11742406]

20. Lamparter T, Carrascal M, Michael N, Martinez E, Rottwinkel G, Abian J. The biliverdin chromophore binds covalently to a conserved cysteine residue in the N-terminus of Agrobacterium phytochrome Agp1. Biochemistry 2004;43:3659–3669. [PubMed: 15035636]

21. Tasler R, Moises T, Frankenberg-Dinkel N. Biochemical and spectroscopic characterization of the bacterial phytochrome of *Pseudomonas aeruginosa*. FEBS J 2005;272:1927–1936. [PubMed: 15819886]

22. Rüdiger W, Thümmler F, Cmiel E, Schneider S. Chromophore structure of the physiologically active form (P_{fr}) of phytochrome. Proc Natl Acad Sci USA 1983;80:6244–6248. [PubMed: 16593380]

23. Sineshchekov VA. Photobiophysics and photobiochemistry of the heterogeneous phytochrome system. Biochim Biophys Acta Bioenerg 1995;1228:125–164.

24. Braslavsky, S. E. (2003) Phytochrome, in Photochromism: Molecules and Systems (Dürr, H., and Bouas-Laurent, H., Eds.) pp 738–755, Elsevier Science BV, Amsterdam, The Netherlands.

25. Yeh KC, Lagarias JC. Eukaryotic phytochromes: Light-regulated serine/threonine protein kinases with histidine kinase ancestry. Proc Natl Acad Sci USA 1998;95:13976–13981. [PubMed: 9811911]

26. Lamparter T, Esteban B, Hughes J. Phytochrome Cph1 from the cyanobacterium *Synechocystis* PCC6803—Purification, assembly, and quaternary structure. Eur J Biochem 2001;268:4720–4730. [PubMed: 11532008]

27. Karniol B, Vierstra RD. The pair of bacteriophytochromes from *Agrobacterium tumefaciens* are histidine kinases with opposing photobiological properties. Proc Natl Acad Sci USA 2003;100:2807–2812. [PubMed: 12604773]

28. Giraud E, Zappa S, Vuillet L, Adriano JM, Hannibal L, Fardoux J, Berthomieu C, Bouyer P, Pignol D, Vermeglio A. A new type of bacteriophytochrome acts in tandem with a classical bacteriophytochrome to control the antennae synthesis in *Rhodopseudomonas palustris*. J Biol Chem 2005;280:32389–32397. [PubMed: 16009707]

29. Martinez-Garcia JF, Huq E, Quail PH. Direct targeting of light signals to a promoter element-bound transcription factor. Science 2000;288:859–863. [PubMed: 10797009]

30. Matsushita T, Mochizuki N, Nagatani A. Dimers of the N-terminal domain of phytochrome B are functional in the nucleus. Nature 2003;424:571–574. [PubMed: 12891362]

31. Oka Y, Matsushita T, Mochizuki N, Suzuki T, Tokutomi S, Nagatani A. Functional analysis of a 450-amino acid N-terminal fragment of phytochrome B in *Arabidopsis*. Plant Cell 2004;16:2104–2116. [PubMed: 15273294]

32. Montgomery BL, Lagarias JC. Phytochrome ancestry. Sensors of bilins and light. Trends Plant Sci 2002;7:357–366. [PubMed: 12167331]

33. Lamparter T, Michael N, Caspani O, Miyata T, Shirai K, Inomata K. Biliverdin binds covalently to *Agrobacterium* phytochrome Agp1 via its ring A vinyl side chain. J Biol Chem 2003;278:33786–33792. [PubMed: 12824166]

34. Quest B, Gärtner W. Chromophore selectivity in bacterial phytochromes: Dissecting the process of chromophore attachment. Eur J Biochem 2004;271:1117–1126. [PubMed: 15009190]

35. Strauss HM, Hughes J, Schmieder P. Heteronuclear solution-state NMR studies of the chromophore in cyanobacterial phytochrome Cph1. Biochemistry 2005;44:8244–8250. [PubMed: 15938613]

36. Kneip C, Hildebrandt P, Schlamann W, Braslavsky SE, Mark F, Schaffner K. Protonation state and structural changes of the tetrapyrrole chromophore during the $P_r \rightarrow P_{fr}$ phototransformation of phytochrome: A resonance Raman spectroscopic study. Biochemistry 1999;38:15185–15192. [PubMed: 10563801]

37. Foerstendorf H, Benda C, Gartner W, Storf M, Scheer H, Siebert F. FTIR studies of phytochrome photoreactions reveal the C=O bands of the chromophore: Consequences for its protonation states, conformation, and protein interaction. Biochemistry 2001;40:14952–14959. [PubMed: 11732915]

38. Borucki B, Otto H, Rottwinkel G, Hughes J, Heyn MP, Lamparter T. Mechanism of Cph1 phytochrome assembly from stopped-flow kinetics and circular dichroism. Biochemistry 2003;42:13684–13697. [PubMed: 14622015]

39. Göller AH, Strehlow D, Hermann G. The excited-state chemistry of phycocyanobilin: A semiempirical study. ChemPhysChem 2005;6:1259–1268. [PubMed: 15942968]

40. Mroginski MA, Murgida DH, von Stetten D, Kneip C, Mark F, Hildebrandt P. Determination of the chromophore structures in the photoinduced reaction cycle of phytochrome. J Am Chem Soc 2004;126:16734–16735. [PubMed: 15612706]

41. Inomata K, Hammam MA, Kinoshita H, Murata Y, Khawn H, Noack S, Michael N, Lamparter T. Sterically locked synthetic bilin derivatives and phytochrome Agp1 from *Agrobacterium tumefaciens* form photoinsensitive P_r- and P_{fr}-like adducts. J Biol Chem 2005;280:24491–24497. [PubMed: 15878872]

42. Tu, S.-L., and Lagarias, J. C. (2005) The phytochromes, in Handbook of Photosensory Receptors (Briggs, W. R., and Spudich, J. A., Eds.) pp 121–149, Wiley VCH, Weinheim, Germany.

43. Vierstra RD. Illuminating phytochrome functions. Plant Physiol 1993;103:679–684. [PubMed: 12231971]

44. Park CM, Shim JY, Yang SS, Kang JG, Kim JI, Luka Z, Song PS. Chromophore–apoprotein interactions in *Synechocystis* sp. PCC6803 phytochrome Cph1. Biochemistry 2000;39:6349–6356. [PubMed: 10828948]

45. Wu SH, Lagarias JC. Defining the bilin lyase domain: Lessons from the extended phytochrome superfamily. Biochemistry 2000;39:13487–13495. [PubMed: 11063585]

46. Fischer AJ, Lagarias JC. Harnessing phytochrome's glowing potential. Proc Natl Acad Sci USA 2004;101:17334–17339. [PubMed: 15548612]

47. Zhao KH, Ran Y, Li M, Sun YN, Zhou M, Storf M, Kupka M, Böhm S, Bubenzer C, Scheer H. Photochromic biliproteins from the cyanobacterium *Anabaena* sp. PCC 7120: Lyase activities, chromophore exchange, and photochromism in phytochrome AphA. Biochemistry 2004;43:11576–11588. [PubMed: 15350144]

48. Gambetta GA, Lagarias JC. Genetic engineering of phytochrome biosynthesis in bacteria. Proc Natl Acad Sci USA 2001;98:10566–10571. [PubMed: 11553807]

49. Frankenberg N, Mukougawa K, Kohchi T, Lagarias JC. Functional genomic analysis of the HY2 family of ferredoxin-dependent bilin reductases from oxygenic photosynthetic organisms. Plant Cell 2001;13:965–978. [PubMed: 11283349]

50. Elich TD, Chory J. Biochemical characterization of *Arabidopsis* wild-type and mutant phytochrome B holoproteins. Plant Cell 1997;9:2271–2280. [PubMed: 9437866]

51. Laemmli UK. Cleavage of structural proteins during the assembly of bacteriophage T4. Nature 1970;227:680–685. [PubMed: 5432063]

52. Berkelman TR, Lagarias JC. Visualization of bilin-linked peptides and proteins in polyacrylamide gels. Anal Biochem 1986;156:194–201. [PubMed: 3526971]

53. Li L, Lagarias JC. Phytochrome assembly—Defining chromophore structural requirements for covalent attachment and photoreversibility. J Biol Chem 1992;267:19204–19210. [PubMed: 1527043]

54. Murphy JT, Lagarias JC. Purification and characterization of recombinant affinity peptide-tagged oat phytochrome A. Photochem Photobiol 1997;65:750–758. [PubMed: 9114754]

55. Southwick PL, Ernst LA, Tauriello EW, Parker SR, Mujumdar RB, Mujumdar SR, Clever HA, Waggoner AS. Cyanine dye labeling reagents—Carboxymethylin-docyanine succinimidyl esters. Cytometry 1990;11:418–430. [PubMed: 2340776]

56. Martinez SE, Wu AY, Glavas NA, Tang XB, Turley S, Hol WG, Beavo JA. The two GAF domains in phosphodiesterase 2A have distinct roles in dimerization and in cGMP binding. Proc Natl Acad Sci USA 2002;99:13260–13265. [PubMed: 12271124]

57. Bower MJ, Cohen FE, Dunbrack RL Jr. Prediction of protein side-chain rotamers from a backbone-dependent rotamer library: A new homology modeling tool. J Mol Biol 1997;267:1268–1282. [PubMed: 9150411]

58. Frisch, M. J., Trucks, G. W., Schlegel, H. B., Scuseria, G. E., Robb, M. A., Cheeseman, J. R., Zakrzewski, V. G., Montgomery, J. A., Jr., Stratmann, R. E., Burant, J. C., Dapprich, S., Millam, J. M., Daniels, A. D., Kudin, K. N., Strain, M. C., Farkas, O., Tomasi, J., Barone, V., Cossi, M., Cammi, R., Mennucci, B., Pomelli, C., Adamo, C., Clifford, S., Ochterski, J., Petersson, G. A., Ayala, P. Y., Cui, Q., Morokuma, K., Malick, D. K., Rabuck, A. D., Raghavachari, K., Foresman, J. B., Cioslowski, J., Ortiz, J. V., Baboul, A. G., Stefanov, B. B., Liu, G., Liashenko, A., Piskorz, P., Komaromi, I., Gomperts, R., Martin, R. L., Fox, D. J., Keith, T., Al-Laham, M. A., Peng, C. Y., Nanayakkara, A., Gonzalez, C., Challacombe, M., Gill, P. M. W., Johnson, B. G., Chen, W., Wong, M. W., Andres, J. L., Head-Gordon, M., Replogle, E. S., and Pople, J. A. (1998) Gaussian 98 (Revision A.9), Gaussian, Inc., Pittsburgh, PA.

59. Duan Y, Wu C, Chowdhury S, Lee MC, Xiong G, Zhang W, Yang R, Cieplak P, Luo R, Lee T, Caldwell J, Wang J, Kollman P. A point-charge force field for molecular mechanics simulations of proteins based on condensed-phase quantum mechanical calculations. J Comput Chem 2003;24:1999–2012. [PubMed: 14531054]

60. van Gunsteren, W. F., Billeter, S. R., Eising, A. A., Hünenberger, P. H., Krüger, P., Mark, A. E., Scott, W. R. P., and Tironi, I. G. (1996) The GROMOS96 Manual and User Guide, VdF Hochsculverlag AG an der ETH Zürich, Zürich, Switzerland.

61. Lindahl E, Hess B, van der Spoel D. GROMACS 3.0: A package for molecular simulation and trajectory analysis. J Mol Model 2001;7:306–317.

62. Humphrey W, Dalke A, Schulten K. VMD: Visual molecular dynamics. J Mol Graphics 1996;14:27–28.33–38.

63. Fiser A, Sali A. Modeller: Generation and refinement of homology-based protein structure models. Methods Enzymol 2003;374:461–491. [PubMed: 14696385]

64. Sarkar HK, Song PS. Nature of phototransformation of phytochrome As probed by intrinsic tryptophan residues. Biochemistry 1982;21:1967–1972. [PubMed: 7082656]

65. Stone, J. (1998) Master's thesis in Computer Science Department, University of Missouri—Rolla.

66. Frishman D, Argos P. Knowledge-based protein secondary structure assignment. Proteins 1995;23:566–579. [PubMed: 8749853]

67. Russell RB, Barton GJ. Multiple protein sequence alignment from tertiary structure comparison: Assignment of global and residue confidence levels. Proteins 1992;14:309–323. [PubMed: 1409577]

68. Thompson JD, Higgins DG, Gibson TJ. CLUSTAL W: Improving the sensitivity of progressive multiple sequence alignment through sequence weighting, position-specific gap penalties, and weight matrix choice. Nucleic Acids Res 1994;22:4673–4680. [PubMed: 7984417]

69. Bashford D, Gerwert K. Electrostatic calculations of the pK_a values of ionizable groups in bacteriorhodopsin. J Mol Biol 1992;224:473–486. [PubMed: 1313886]

70. Spassov VZ, Luecke H, Gerwert K, Bashford D. pK_a calculations suggest storage of an excess proton in a hydrogen-bonded water network in bacteriorhodopsin. J Mol Biol 2001;312:203–219. [PubMed: 11545597]

71. Falk, H. (1989) The Chemistry of Linear Oligopyrroles and Bile Pigments, pp 621, Springer-Verlag, Vienna, Austria.

72. Ho YS, Burden LM, Hurley JH. Structure of the GAF domain, a ubiquitous signaling motif, and a new class of cyclic GMP receptor. EMBO J 2000;19:5288–5299. [PubMed: 11032796]

73. Martinez SE, Bruder S, Schultz A, Zheng N, Schultz JE, Beavo JA, Linder JU. Crystal structure of the tandem GAF domains from a cyanobacterial adenylyl cyclase: Modes of ligand binding and dimerization. Proc Natl Acad Sci USA 2005;102:3082–3087. [PubMed: 15708973]

74. Bischoff M, Hermann G, Rentsch S, Strehlow D. First steps in the phytochrome phototransformation: A comparative femtosecond study on the forward (Pr → Pfr) and back reaction (Pfr → Pr). Biochemistry 2001;40:181–186. [PubMed: 11141069]

75. Heyne K, Herbst J, Stehlik D, Esteban B, Lamparter T, Hughes J, Diller R. Ultrafast dynamics of phytochrome from the cyanobacterium *Synechocystis*, reconstituted with phycocyanobilin and phycoerythrobilin. Biophys J 2002;82:1004–1016. [PubMed: 11806940]

76. Murphy JT, Lagarias JC. The phytofluors: A new class of fluorescent protein probes. Curr Biol 1997;7:870–876. [PubMed: 9382811]

77. Schirmer T, Bode W, Huber R. Refined three-dimensional structures of two cyanobacterial C-phycocyanins at 2.1 and 2.5 Å resolution. A common principle of phycobilin–protein interaction. J Mol Biol 1987;196:677–695. [PubMed: 3119857]

78. Duerring M, Schmidt GB, Huber R. Isolation, crystallization, crystal structure analysis, and refinement of constitutive C-phycocyanin from the chromatically adapting cyanobacterium *Fremyella diplosiphon* at 1.66 Å resolution. J Mol Biol 1991;217:577–592. [PubMed: 1899708]

79. Kuramitsu S, Hamaguchi K, Miwa S, Nakashima K. Ionization of the catalytic groups and tyrosyl residues in human lysozyme. J Biochem 1980;87:771–778. [PubMed: 7390961]

80. Bashford D, Karplus M. pK_a's of ionizable groups in proteins: Atomic detail from a continuum electrostatic model. Biochemistry 1990;29:10219–10225. [PubMed: 2271649]

81. Inoue M, Yamada H, Hashimoto Y, Yasukochi T, Hamaguchi K, Miki T, Horiuchi T, Imoto T. Stabilization of a protein by removal of unfavorable abnormal pK_a: Substitution of undissociable residue for glutamic acid-35 in chicken lysozyme. Biochemistry 1992;31:8816–8821. [PubMed: 1390669]

1. Martinez SE, Wu AY, Glavas NA, Tang XB, Turley S, Hol WG, Beavo JA. The two GAF domains in phosphodiesterase 2A have distinct roles in dimerization and in cGMP binding. Proc Nat Acad Sci USA 2002;99:13260–5. [PubMed: 12271124]

2. Tasler R, Moises T, Frankenberg-Dinkel N. Biochemical and spectroscopic characterization of the bacterial phytochrome of Pseudomonas aeruginosa. FEBS J 2005;272:1927–36. [PubMed: 15819886]

3. Davis SJ, Vener AV, Vierstra RD. Bacteriophytochromes: phytochrome-like photoreceptors from nonphotosynthetic eubacteria. Science 1999;286:2517–20. [PubMed: 10617469]
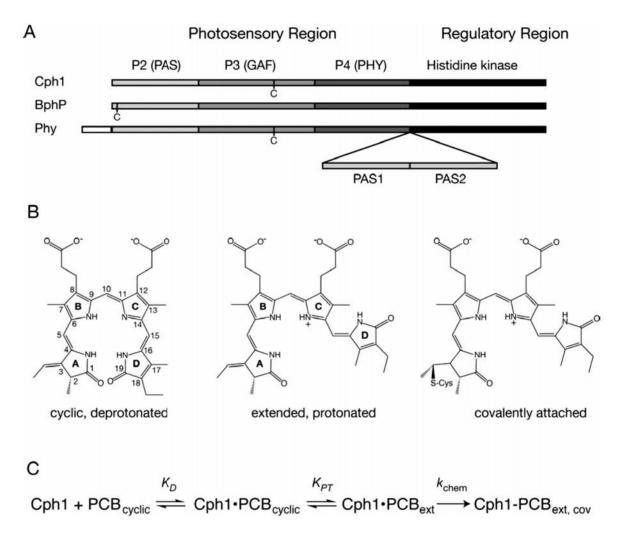
Figure 1.
Domain structure, chromophore configuration, and assembly of phytochromes. (A) Domain organization of the Cph1, BphP, and Phy subfamilies. The N-terminal photosensory region contains the P2 PAS domain, the P3 GAF bilin lyase domain, and the P4 PHY domain. Plant phytochromes (Phy) also possess a Ser/Thr-rich N-terminal P1 domain. The C-terminal regulatory region of these phytochromes contains a domain homologous to histidine kinase transmitter modules. Plant phytochrome C termini possess an additional inserted region that contains two additional PAS domains (labeled PAS1 and PAS2). Cys sites of covalent attachment to the bilin chromophore are indicated. (B) Conformations of the free chromophore precursor phycocyanobilin (PCB) and its protonated form during assembly. Rings are labeled in bold, and the carbons of the ring system are numbered. (Left) A cyclic, deprotonated C5 *Z,syn*, C10 *Z,syn*, C15 *Z,syn* configuration of the initially bound PCB is shown. (Center) Upon protonation of the ring system, PCB adopts a more extended conformation, here shown as C5 *Z,syn*, C10 *Z,syn*, C15 *Z,anti*. (Right) The covalent attachment of PCB to Cph1 results in a covalent thioether linkage to Cys_{259} with *R* stereochemistry (*16*). (C) Assembly reaction of PCB with wild-type phytochrome Cph1 is shown (*38*). After initially binding in a cyclic conformation, PCB becomes protonated and adopts a more extended conformation ("ext"). The thioether linkage is then formed ("ext, cov"). K_D, initial binding constant for PCB and apoCph1; K_{PT}, equilibrium constant for proton transfer and concomitant chromophore rearrangement; k_{chem}, rate constant for covalent attachment.
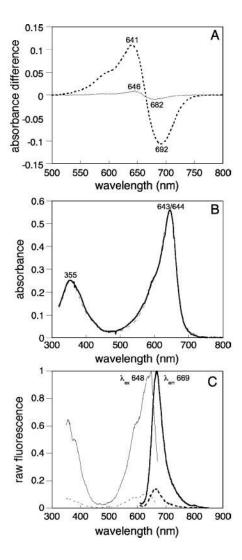
Figure 2.
Spectroscopic and fluorescent properties of PCB adducts of recombinant *Arabidopsis* PhyB (N450) wild-type (- - -) and $Y_{276}H$ (—) proteins. (A) Absorbance difference spectra were normalized for equal absorbance at the blue band, demonstrating that the amount of photoconversion is highly reduced for the $Y_{276}H$ mutant compared to the wild-type. (B) Absorbance spectra normalized to the blue band, showing that there is little difference in the bilin configuration or λ_{max} between the wild-type and Tyr_{276} mutant. (C) Fluorescence excitation (thin line) and emission (thick line) spectra of the wild type and mutant (samples were adjusted to have equal absorbance at 648 nm).
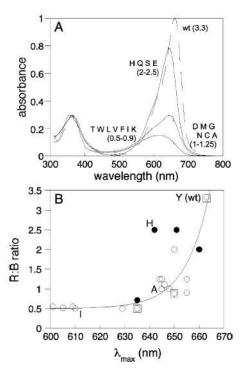
Figure 3.
Substitution mutants at Tyr_{176} and Glu_{189} alter chromophore configuration. (A) Absorbance spectra were normalized to the blue band. Tyr_{176} substitutions exhibiting various ranges of R/B ratios are shown with representative absorbance spectra. The spectra shown are wild type, $Y_{176}H$, $Y_{176}A$, and $Y_{176}I$. (B) A plot of the R/B ratio versus the maximal absorbance wavelength for the long wavelength band is shown for the wild-type and mutant proteins with substitutions at Tyr_{176} (○) or Glu_{189} (□). Proteins whose spectra are shown in A are indicated in one-letter code. Substitutions at Tyr_{176} which resulted in fluorescence, are shown in •, while the wild type and other substitutions are shown as ○ and were fitted to a smooth hyperbolic function (—).
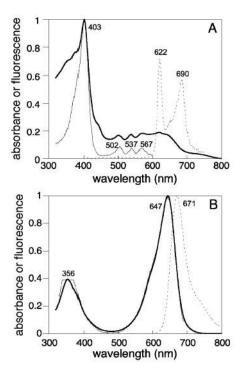
Figure 4.
$Y_{176}R$ mutant protein affects chromophore-binding specificity. (A) Absorbance (thick solid line), fluorescence excitation (thin solid line), and fluorescence emission (dashed line) spectra of the $Y_{176}R$ mutant Cph1Δ protein. The multiple fluorescence excitation peaks and sharp fluorescence emission peak at approximately 620 nm are characteristic of a porphyrin (*71*), while the broader absorbance around 620 nm is indicative of a second population with bound bilin. (B) Absorbance and fluorescence excitation and emission spectra of the $Y_{176}H$ mutant Cph1Δ protein for comparison. Spectra are the same as in A.
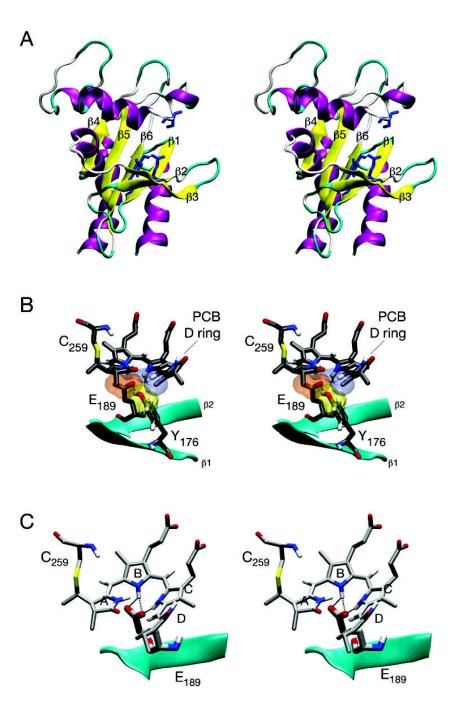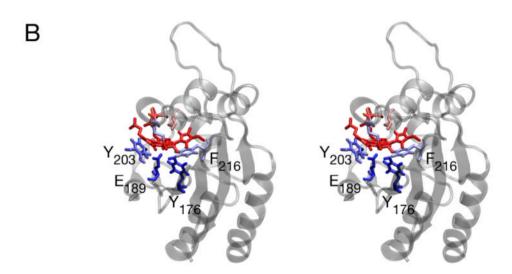
Figure 5.
Stereoviews of the Cph1 bilin lyase domain homology model. (A) Proposed Cph1 bilin lyase fold shows a central twisted β sheet, with Tyr_{176} and Glu_{189} (blue) on adjacent strands ($\beta1$ and $\beta2$, respectively). Both side chains point up into the proposed chromophore-binding pocket, with the nucleophilic Cys_{259} (blue) above Tyr_{176} and Glu_{189}. β strands are numbered on the basis of their position in the sequence starting from the N terminus. (B) PCB is shown attached to Cys_{259}, with Tyr_{176} and Glu_{189} lying below the chromophore (colors: C, gray; H, white; N, blue; O, red; and S, yellow). For Tyr_{176} and Glu_{189}, atoms within 3.4 Å of PCB are also shown as solvent-accessible surfaces (Tyr_{176}, yellow; and Glu_{189}, orange). PCB atoms within 3.4 Å of Tyr_{176} are shown as a solvent-accessible surface (light blue). (C) Interactions between
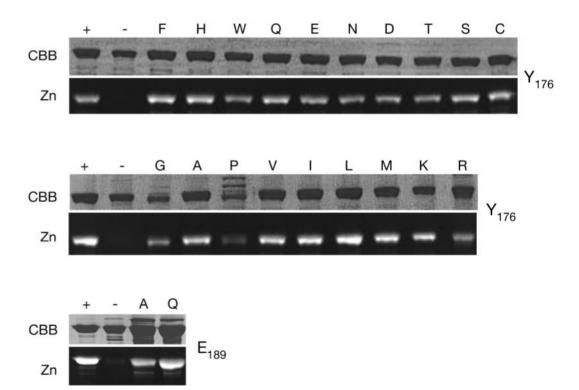
Glu$_{189}$ and PCB. The Glu$_{189}$ side chain is hydrogen-bonded to the B/C-ring system of the protonated chromophore, stabilizing the positive charge. The rings of PCB are labeled for clarity.

A

```
Cph1    -------------------N-LRDFYDVIVEEVRRMTGFDRVMLYRFDENNHGDVIAED
1MC0N   YTDHDRKILQLCGELF---DLDATSLQLKVLQYLQQETQATHCCLLLVSED-N-LQLSCK
1MC0C   ----------------FTHLDDVSVLLQEIITEARNLSNAEICSVFLLD-Q---NELVAK

Cph1    KRD-DMEPY-L---GLHYPESDIPQPARRLFIH----NPIRVIPDVYGVAVPLTPAVNPS
1MC0N   -VIGDK-VLGE---EVSF--PL-TM-G--RLGQVVEDKQCIQL----KD-----------
1MC0C   -VFDGG-VVDDESYEIRI--PA-DQ-G--IAGHVATTGQILNIPDAYAH----P------

Cph1    TNRAVDLT-ESILRSAY-HCHLTYLKNMGVGASLTISLIK-DG--HLWGLIACHHQTPKV
1MC0N   -------LTSDDVQQLQ-NML--GC---ELQAMLCVPVISRATDQVVALACAF-NKLG--
1MC0C   ------LFY---RG-VDDST---GF---RTRNILCFPIKN-ENQEVIGVAELV-NKIN--

Cph1    IPFELRKACEFFGRVVFSNISAQEDT---------------
1MC0N   -GDFFTDEDEHVIQHCFHY---TG-TVLTST--------LA
1MC0C   -GPWFSKFDEDLATAFSIYCGISI-AHSLLYKKVNEAQY--
```

B
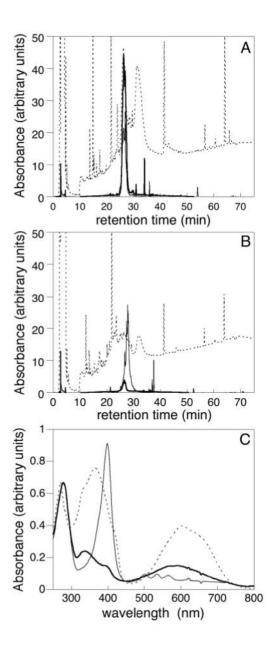
Supplemental Figure 1.
The Cph1 GAF domain and chromophore-binding pocket. (A) Sequence alignment of the Cph1 GAF domain and the two GAF domains of mouse phosphodiesterase 2A (PDB code 1MC0: (*1*)) with Tyr_{176} and Glu_{189} in red. (B) Residues within 3 Å of PCB (red) are continually colored by identity ranging from dark blue, absolutely conserved, to bright red, variable using an alignment of Cph1, the five phytochrome proteins in the *A. thaliana* genome, and BphP proteins from *P. aeruginosa* and *Deinococcus radiodurans (2,3)*.

Supplemental Figure 2.
SDS/PAGE (CBB) and zinc-blot (Zn) analysis of Cph1Δ mutant proteins as PCB adducts. 3 μg of total protein was run per lane except for $Y_{176}P$ (30 μg). Wildtype holoCph1Δ (+) and apoCph1Δ (−) are shown for each gel. The remaining lanes are labeled with the amino acid substituted for Tyr at position 176 (top two panels) or for Glu at position 189 (bottom panel). $Y_{176}P$ is largely insoluble; therefore a ten-fold excess of total protein was loaded in order to demonstrate its presence. The Cph1Δ proteins all migrate with a relative molecular mass of 60 kDa.

Supplemental Figure 3.
Analysis of chromopeptides. Peptides derived from wildtype (A) and $Y_{176}R$ (B) Cph1 were analyzed by HPLC: 220 nm (dashed), 400 nm (porphyrin, thin line), and 650 nm (bilin, thick line). (C) Absorbance spectra for wildtype (dashed) and $Y_{176}R$ (peak 1, thick line; peak 2, thin line) chromopeptides.

Table 1

Spectral Properties of PCB–Cph1Δ Holoproteins[a]

Cph1	λ_{max}[b]	R/B[c]	% ΔΔA[d]	Φ_f[e]	λ_{ex}[f]	λ_{em}[f]
wild type	365, 663	3.33	100	0.005	356, 647	676
$Y_{176}S$	359, 650	2.0	34	nd[g]	nd[g]	nd[g]
$Y_{176}T$	364, 655	0.9	13	nd[g]	nd[g]	nd[g]
$Y_{176}W$	365, 635	0.71	0.3	0.077	356, 647	671
$Y_{176}H$	355, 645	2.5	1.9	0.145	356, 647	671
$Y_{176}Q$	357, 651	2.5	1.6	0.121	355, 649	678
$Y_{176}E$	365, 660	2.0	7.5	0.086	359, 664	681
$Y_{176}K$	356, 629	0.5	0.5	nd[g]	nd[g]	nd[g]
$Y_{176}I$	364, 610	0.5	0.2	nd[g]	nd[g]	nd[g]
$Y_{176}F$	364, 605	0.52	3.0	nd[g]	nd[g]	nd[g]
$Y_{176}L$	362, 609	0.55	0.2	nd[g]	nd[g]	nd[g]
$Y_{176}V$	362, 601	0.55	0.9	nd[g]	nd[g]	nd[g]
$Y_{176}A$	364, 645	1.0	9.5	nd[g]	nd[g]	nd[g]
$Y_{176}C$	364, 648	1.0	5.0	nd[g]	nd[g]	nd[g]
$Y_{176}N$	357, 646	1.11	4.7	nd[g]	nd[g]	nd[g]
$Y_{176}D$	364, 655	1.25	7.9	nd[g]	nd[g]	nd[g]
$Y_{176}M$	364, 645	1.25	5.6	nd[g]	nd[g]	nd[g]
$Y_{176}G$	365, 644	1.25	3.7	nd[g]	nd[g]	nd[g]
$E_{189}A$	353, 635	0.5	4.0	nd[g]	nd[g]	nd[g]
$E_{189}Q$	366, 650	0.88	10	nd[g]	nd[g]	nd[g]

[a]Wild-type and mutant Cph1Δ holoproteins were purified as described in the Materials and Methods after expression in *E. coli* cells synthesizing PCB (*48*). Reported values are for proteins in the P_r form. $Y_{176}P$ and $Y_{176}R$ are not included in the table. $Y_{176}P$ was poorly expressed and was not characterized in detail. As shown in Figure 4, $Y_{176}R$ primarily bound to a porphyrin, with absorbance maxima at 403, 503, 539, 568, and 623 nm, fluorescence excitation maxima at 402, 502, 537, and 567 nm, and fluorescence emission maxima at 622, 650, and 690 nm.

[b]Two values are presented. The first is the wavelength of maximal absorbance for the blue band (350–400 nm), while the second is the wavelength of maximal absorbance for the red band (600–700 nm). All values are in nanometers.

[c]R/B ratio is defined as the ratio of the peak absorbance value of the red band divided by that of the blue band.

[d]Percent photoconversion efficiency was determined by subtracting the P_{fr} spectrum from the P_r spectrum, subtracting the resulting difference minimum from the difference maximum, and normalizing to the wild type as 100%. Spectra were normalized to the blue band absorbance prior to the calculation.

[e]Fluorescence quantum yield.

[f]Maximal fluorescence excitation (λ_{ex}) and emission (λ_{em}) wavelengths are presented as instrument-corrected values in nanometers.

[g]nd = not determined.

Supplemental Table 1

Spectral properties of phytochrome constructs[a]

Protein	Construct	Bilin	λ_{max}	%$\Delta\Delta A$	Φ_f	λ_{ex}	λ_{em}
Cph1Δ	wildtype	PCB	365, 663	100	0.005	356, 647	676
"	Y$_{176}$H	PCB	365, 635	1.9	0.145	356, 647	671
"	Y$_{176}$W	PCB	355, 642	0.3	0.077	356, 647	671
"	Y$_{176}$Q	PCB	357, 651	1.6	0.121	355, 649	678
"	Y$_{176}$E	PCB	365, 660	7.5	0.086	359, 654	681
"	wildtype	PΦB	380, 675	100	0.002	383, 647	688
"	Y$_{176}$H	PΦB	376, 655	2.0	0.067	387, 650	683
"	Y$_{176}$W	PΦB	382, 656	0	0.080	385, 649	682
"	Y$_{176}$Q	PΦB	380, 661	0.63	0.071	388, 650	685
"	Y$_{176}$E	PΦB	377, 672	0.3	0.042	390, 668	692

[a]Spectral properties of various phytochrome constructs were determined as described in Table 1. Units for wavelengths are in nm. Fluorescence quantum yield is a dimensionless quantity.

[b]n.d., not determined.